Three-phase coupled analysis about seismic behavior of embankment under cold snowy condition

T. Matsumaru
Railway Technical Research Institute, Structural Technology Division, Japan
S. Kawajiri
Kitami Institute of Technology, Department of Civil and Environmental Engineering, Japan

ABSTRACT: To investigate the seismic behavior of embankments under cold snowy conditions, a series of numerical simulations were conducted. For the numerical simulations, a soil-water-air coupled analysis was employed to consider the change in the boundary conditions and permeability of pore water and air, caused by freezing and thawing. It was revealed that the seismic resistance of embankments decreased at the end of thawing and are similar to embankments affected by severe rainfall, especially in the case of low embankment heights. The reason of the decrease in the seismic resistance was estimated to be the change in the boundary conditions of pore water and pore air at the surface of the embankment.

1 INTRODUCTION

In the snowy regions, damage to the embankments was reported at the time of a thaw. The mechanism of the damage is estimated to be attributable to the increase in the degree of saturation in the embankment due to the seepage of the thaw water. The seismic resistance of the embankment decreases with the increase in the degree of saturation. Indeed, during the 2004 Niigata-ken Chuetsu earthquake in Japan, several railway and road embankments collapsed. The main reason of such damages was the increase in the degree of saturation caused by the typhoon before the earthquake (Morishima et al 2005; Matsumaru and Uzuoka 2016). At the time of a thaw, not only the increase in the degree of saturation but also the change in the boundary condition of pore water and air at the surface of the embankment affects its seismic resistance. However, no precise evaluation with a focus on such change in boundary conditions has yet to be conducted.

In this paper, a series of the numerical simulations were conducted to evaluate the seismic resistance of the embankment at the time of a thaw. For the numerical technique, the three-phase (soil, water, and air) coupled analysis was applied. The conventional constitutive model for unsaturated sandy soil was also employed. In the simulations, the infiltration of thaw water and the change in the boundary conditions of pore water and air were considered.

2 NUMERICAL TECHNIQUE

In this study, the governing equations for three phase mixtures (soil particle, pore water, and pore air) were adopted (Uzuoka and Bojra 2012). The governing equations were formulated based on the following assumptions:

1) The conditions are isothermal;
2) The soil particles are incompressible;
3) The mass exchange among phases can be neglected;
4) The material time derivative of relative velocities and the advection terms of pore fluids to the soil skeleton can be neglected.

The isothermal condition means that the freeze-thaw process is not considered, and its influence is considered in the boundary conditions for three phases and the permeability coefficients of pore water and the air.

The governing equations consist of the momentum balance equations of mixtures and the mass and momentum balance equations of pore water and air.

The governing equations consist of the momentum balance equations of mixtures and the mass and momentum balance equations of pore water and air.

The weak forms were implemented in finite element formulation. The Newmark implicit scheme is used for time integration. The primary variables are the second-order material time derivatives of the displacement of the soil skeleton, pore water pressure and pore air pressure.

The weak forms are linearized and solved by the Newton-Raphson method iteratively at each time step. In the finite element formulation, Galerkin

method and isoparametric 8-node elements are used. The soil skeleton displacement and the fluid pressures are approximated at 8 nodes and 4 nodes respectively to satisfy the discrete LBB conditions for the locally undrained case.

For the constitutive equation for liquefiable sand, a cyclic elasto-plastic model (Matsumaru and Uzuoka 2014a) was applied. This constitutive model was formulated on the following assumptions:

1) The infinitesimal strain theory;
2) The elasto-plastic theory;
3) The non-associated flow rule and the Cam-clay type plastic potential function;
4) The non-linear kinematic hardening rule (Armstrong and Fredrick, 1966) and the dependency of hardening parameters on the amount of plastic strain.

The influence of the freeze-thaw process for the constitutive equation is not considered for the simplicity.

For the soil water characteristic curve, the logistic function model proposed by Sugii et al. (2002) was adopted.

In this study, the skeleton stress was applied as effective stress of unsaturated soil. The skeleton stress is expressed as

$$(-\boldsymbol{\sigma}') = (-\boldsymbol{\sigma}) - p^a \mathbf{I} + s^w \left(p^a - p^w\right)\mathbf{I} \tag{1}$$

where $\boldsymbol{\sigma}'$ is the skeleton stress tensor, p^w and p^a is the pore water pressure and air pressure, and s^w is the degree of water saturation. Stress is defined as positive in extension and pressures are defined as positive in compression.

Using these numerical techniques, we succeeded in reproducing the experimental results well under various stress conditions (Matsumaru and Uzuoka 2014a; 2014b) and the model was applied to simulations treating the liquefaction of the ground and embankment (Matsumaru and Uzuoka 2016).

3 ANALYTICAL CONDITIONS

3.1 *Analytical model*

Figure 1 shows the finite element model of an embankment and the ground. The dimension of the embankment was 10 m in the width of the top, 1:1.5 in the gradient. The height of the embankment is considered as 4 m and 2 m. The water level was set at the surface of the ground. For the simplicity, a freeze and a thaw at the surface of the ground were neglected. In this model, we installed horizontal wide elements, which behave as a free field at both edges of the model to decrease the influence of the reflected wave from the edges. The boundary conditions of the pore water and air are mentioned in 3.3.

3.2 *Soil properties of embankment and ground materials*

For the embankment material, the sandy soil obtained at the embankment damaged in Niigata-ken Chuetsu Earthquake which occurred in 2004 (Morishima et al. 2005) was considered. The particle density G_s is 2.629, 50% diameter on the grain size diagram D_{50} is 0.134 mm, the uniformity coefficient U_c is 11.65, and the fine fraction particle content F_c is 23.3%. The initial dry density was about 1.29 g/cm^3 and the degree of compaction D_c was 87 %. The elasto-plastic constitutive model mentioned in Section 2 was applied.

Unsaturated cyclic triaxial tests (Matsumaru et al. 2015) were conducted for the specimens with different value of initial suction. The material parameters were determined to reproduce these tests (Matsumaru et al. 2015). Table 1 shows the calibrated material parameters of the constitutive model and soil water characteristic curve.

Figure 2 shows the time histories of the pore water pressure of the cyclic triaxial tests and their numerical simulations.

Table 1. Material parameters of Inagi sand.

Parameters	
Elasto-plastic model parameters	
Bulk modulus (K^*)	1349.0
Shear modulus (G^*)	622.0
Nonlinear hardening parameter (a_0, a_1, C_f)	1500, 30, 5000
Nonlinear hardening parameter (b)	-1.331
Critical state stress ratio (M_m)	1.331
Coefficient of dilatancy (D)	0.05
Yield function parameter (k)	0.05
SWCC parameters	
Maximum degree of saturation (s_s^w)	0.962
Minimum degree of saturation (s_r^w)	0.265
LG model parameter (a_{lg}, b_{lg}, c_{lg})	10.0, -2.0, 0.02
Physical parameters of water and air	
Real density of air (ρ_{0s}^{aR})	1.23×10^{-3} t/m^3
Bulk modulus of water (K^w)	1.0×10^{6}kPa
Gas parameter (M^a)	1.21×10^{-5}s^2/m^2

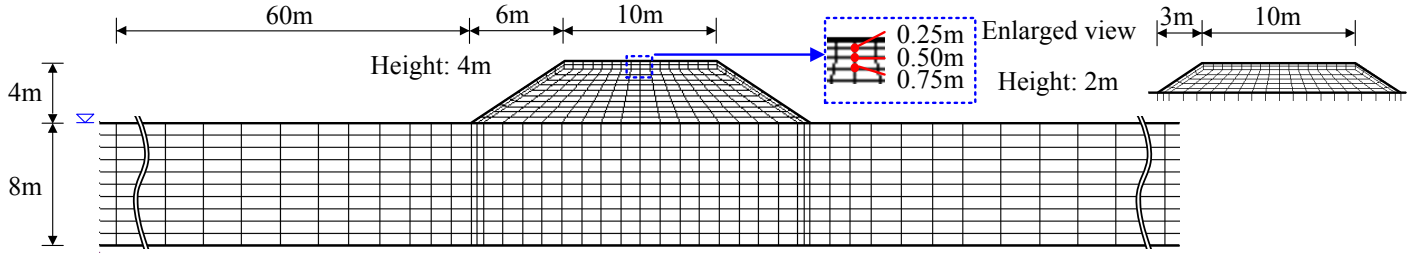

Figure 1. Analytical model

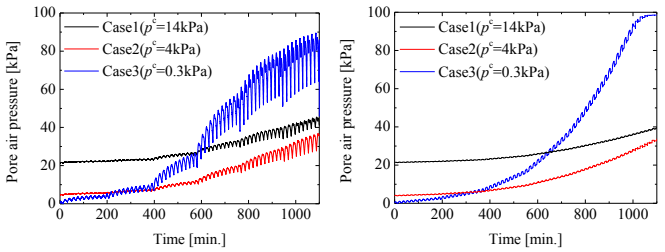

(a) Experiment (b) Simulation

Figure 2. Experimental and numerical results of unsaturated triaxial tests (Matsumaru et al 2015).

The model well reproduced the overall tendency of the test results of each case. In Case 3, the pore water pressure increased largely affected by cyclic loading. However, the amount of increase of the pore water pressure reduced in Cases 1 and 2.

The ground was supposed to be an alluvial clay layer with 120 m/s in shear wave velocity. The cyclic elasto-plastic model was also applied to the ground. However, the dilatancy parameter was set as zero to avoid the occurrence of liquefaction.

3.3 *Soil properties of embankment and ground materials*

Kawajiri et al (2016) conducted the field measurement of an existing embankment in the season of a freeze and a thaw. They measured the temperature and the water content in the embankment, the frozen depth, and the N_d value obtained by the dynamic cone penetration test. Figure 3 shows the illustration of the measured results in the period of a freeze and a thaw. In the period of a freeze, the frozen region was developed due to the decrease in the temperature in the embankment. The permeability of this region became smaller and the N_d value increased dramatically compared to the value before the freeze. However, in the period of the thaw, a thaw occurred and the seepage flow due to the snowmelt was observed at the surface of the embankment. Therefore, the water content at the boundary with the frozen region increased rapidly. Furthermore, the N_d value in the thaw region decreased largely.

The analytical cases and their boundary conditions were determined based on their field measurement. Figure 4 shows the cases of analyses and their boundary conditions. For two embankments with different heights, seismic response analyses were performed after the conditions affected by the rainfall, a freeze or a thaw were evaluated by the seepage analyses. In Case 1, a steady condition was considered, in which the annual rainfall recorded at JAM Kitami (i.e. 790 mm/year) was assumed for three years. In the seepage and dynamic response analyses, at the surface of the embankment, the flow quantity at each node was based on the rainfall record even though this boundary becomes permeable when the pore water pressure is zero. As boundary conditions for the pore air pressure, air drainage was allowed at the surface of the embankment.

In Case 2, a period of the freeze for three months after Case 1 was assumed. In this period, the seepage of rainfall did not occur, and the inner part of the embankment was assumed to be in frozen conditions. In the numerical simulation, the surface of the embankment was assumed to be frozen to a depth of 50 cm, so the permeability coefficient of the pore water and air for the frozen region were 10,000 times smaller than that of the unfrozen region.

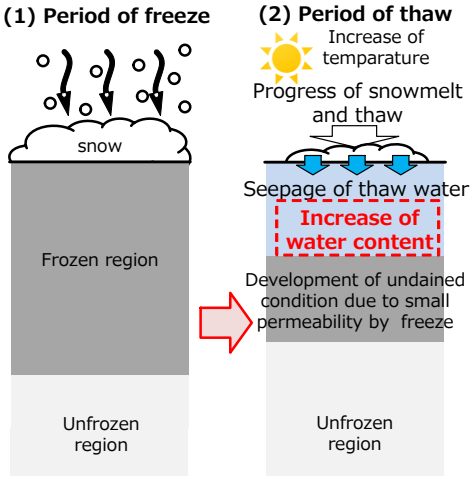

Figure 3. Illustration of field measurement at existing embankment in period of freeze and thaw

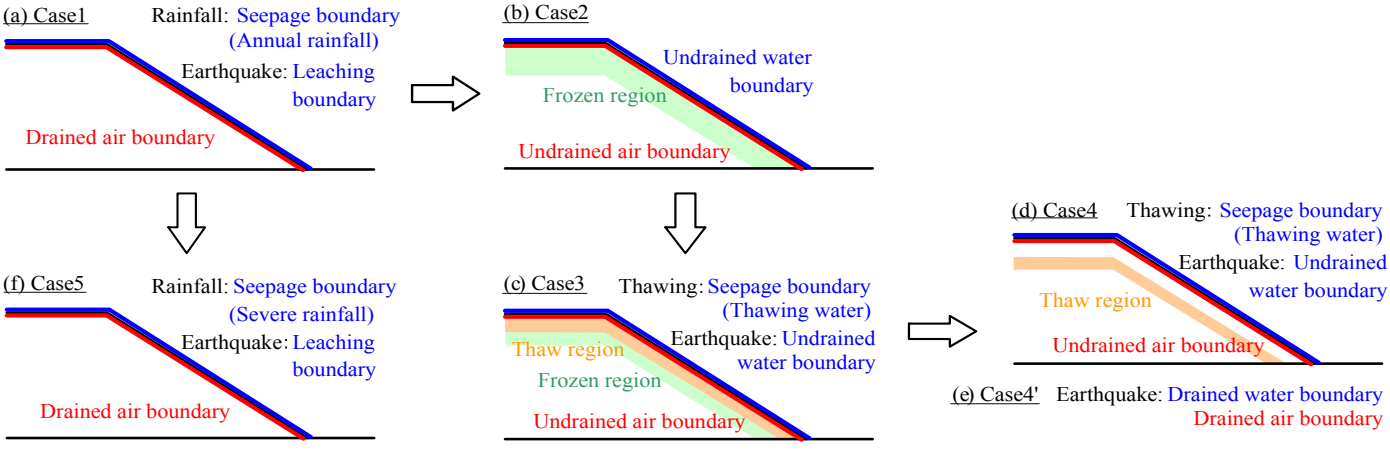

Figure 4. Analytical cases and boundary conditions for pore water and air

For the constitutive equation for the frozen region, the material parameters a_1 was changed from 30 to 1500, to avoid the decrease of hardening parameter for maintaining the skeleton stress. The change of soil water characteristic curve was not considered for the frozen region. Under these conditions, the seepage analysis was conducted under the impermeable boundary condition of pore water and air at the surface of the embankment. The seismic response analysis was not conducted in this case.

In Cases 3 and 4, it was assumed that the thaw occurred for twenty days. Figure 5 shows the time histories applied of the change in the frozen depth and the thickness of snow at the surface of the embankment. It was considered that the thickness of the snow, the density of which was assumed to be 0.3 cm^3/g became zero due to its seepage into the embankment for twenty days. It was assumed that the permeability coefficient of the pore water and air at the first and second layers of the surface increases gradually in this period as is shown in the time history of Figure 5. Cases 3 and 4 represent the situations ten days and twenty days after the thaw started respectively. In this period, the impermeable condition was considered for the pore air and the water in the seismic response analysis. Case 4' was also considered to make a comparison with Case 4 by analyzing the situation when the permeable conditions of pore water and pore air were satisfied.

In Case 5, an embankment affected by severe rainfall was assumed. In this case, as shown in Figure 6, a rainfall whose repeatable provability was 100 years, which is prescribed in the Japanese railway design standard of earth structure (RTRI 2007) was applied. After the seepage analysis using this rainfall, the seismic response analysis was performed.

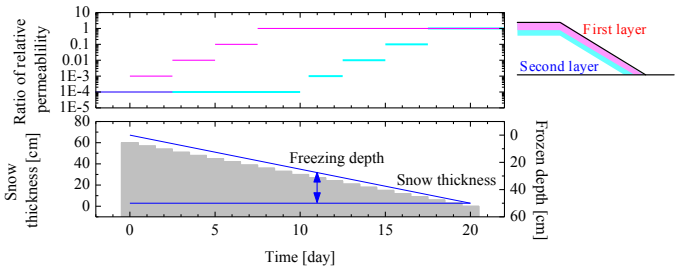

Figure 5. Applied change in snow thickness, frozen depth and relative permeability coefficients for pore water and air used in seepage analysis of Cases 3 and 4

3.4 *Inputted motion*

Figure 7 shows the time history of the ground motion used in the seismic response analysis. The maximum acceleration was 567 gal. This motion was set at the bottom of the finite element model as shown in Figure 1. A time integration step of 0.002 second was adopted for 200 seconds.

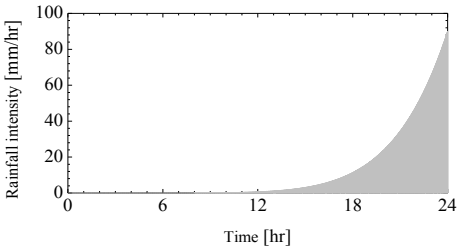

Figure 6. Time history of rainfall used in analysis of Case 5 (RTRI 2007)

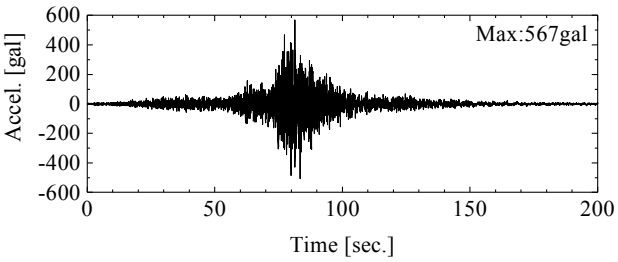

Figure 7. Time history of inputted motion

The coefficients β and γ for the Newmark implicit time integration were 0.6 and 0.3025 respectively.

4 RESULTS AND DISCUSSIONS

4.1 *Stress condition of embankment before earthquake*

Figure 8 shows the distributions of the degree of saturation, suction and mean skeleton stress in the embankment 2 m in height obtained by seepage analysis before earthquake. The mean skeleton stress p' is expressed as:

$$-p' = -tr\sigma'/3 \quad (2)$$

In Case 1, the degree of saturation in the embankment became almost 1.0 at the boundary with the ground affected by the annual rainfall, because the permeability of the ground was smaller than that of the embankment. Compared to the result of this case, the degree of saturation in Cases 3 and 4 increased slightly since the seepage flow occurred due to the thaw at the surface of the embankment. Therefore, the decrease of suction occurred. In Case 5, degree of saturation increased dramatically at the surface of the embankment due to the infiltration of heavy rainfall.

The distributions of the mean skeleton stress showed small differences among cases except Case 5. The skeleton stress is evaluated by two values, the net stress and the suction.

The stress in the embankment would largely depend on the net stress, so the differences among cases became small. In Case 5, the mean skeleton stress at the surface showed a smaller value due to the increase in the degree of saturation.

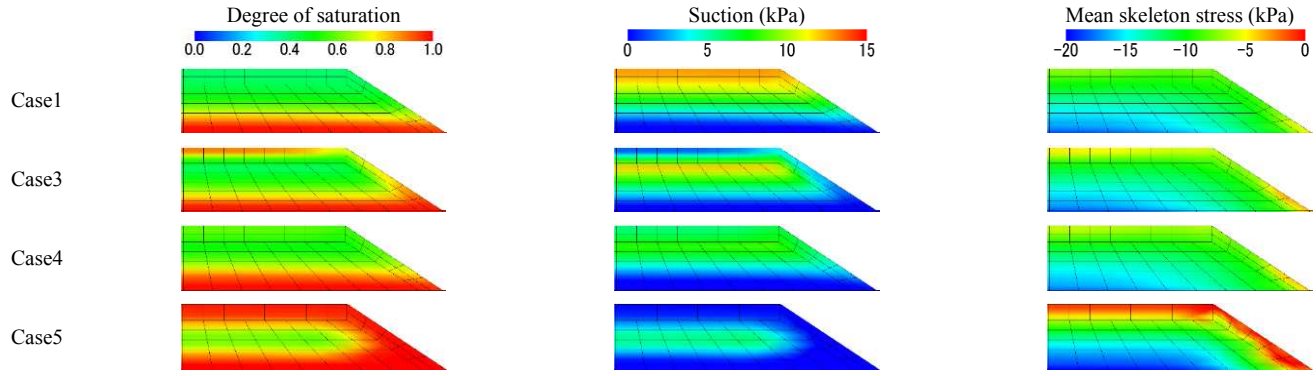

Figure 8. Distribution of degree of saturation, suction, and mean skeleton stress obtained by seepage analyses

4.2 *Settlement of embankment*

Figure 9 shows the settlement of the embankment after shaking for five cases. These figures were drawn by connecting the nodal coordinates after the earthquake, from the centre of the surface to the toe on the right side. The nodal coordinates after the earthquake were obtained by adding the residual displacements to the initial coordinates.

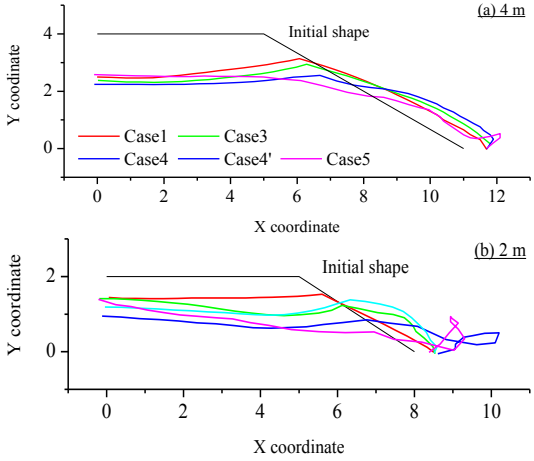

Figure 9. Deformation of embankment after earthquake

Seeing the results with our attention the embankment 4 m in height, the deformed shape for each case did not show large differences at the centre of the embankment. On the other hand, the deformation from the shoulder to the toe differed in each case. In the analysis of Case 4, at the end of the thaw, large deformation was shown, even though the amount of the deformation was smaller than that of Case 5.

The deformation of the embankment 2 m in height was more largely different among cases than that of the embankment 4 m in height. Particularly, the embankments in Cases 4 deformed as largely as that in Case 5, in terms of the settlement of the shoulder and the spread deformation of the toe. This indicated that the decrease in the seismic resistance at the end of the thaw was almost the same as that after the heavy rainfall. However, the deformation shown in Cases 3 and 4 was smaller than that in Cases 4 and 5. The existence of the frozen region and the undrained boundary conditions for pore water and air would affect the degree of deformation caused by the earthquake.

4.3 *Differences of dynamic behaviour among cases*

To clarify the reasons that the simulation of Case 4 2 m in height showed large deformation of the embankment, the dynamic behavior among cases were compared. Figure 10 shows the distributions of the mean skeleton stress and the accumulated strain. The accumulated strain ε_d is defined as:

$$\varepsilon_d = \|\mathbf{e}\| \qquad \mathbf{e} = \boldsymbol{\varepsilon} - \frac{1}{3}\varepsilon_v \tag{1}$$

where ε_d is volumetric strain. These figures contain the results of the simulation of the embankment with 2 m in height for Cases 1, 3, 4 and 5, and the embankment with 4m for Case 4. The distributions of the mean skeleton stress were obtained at 90 second and at the end of the earthquake (i.e.at 200 second), and the accumulated strain was at the end. The mean skeleton stress at 90 second in Cases 4 and 5 showed large decrease though the stress in Case 1 was maintained. However, the mean skeleton stress in Case 3, where the thaw region did not perfectly disappear, was maintained. At the end of the earthquake, the mean skeleton stress in Case 4 showed still small value though that in Case 5 recovered. Affected by the thawing region, the undrained pore water and air condition at the surface of the embankment would cause the decrease and the delay of recovery of the skeleton stress.

The color ranges of the accumulated strain were different between Cases 1 and 3, and Cases 4 and 5. Large strain appeared at the toe of the embankment in Cases 4 and 5. These results indicated that the seismic resistance of the embankment when thawing almost finished became as low as that after heavy rainfall. However, the seismic resistance in Case 3, where thawing is progressing, was not reduced because the surface of the embankment was still stiff due to freeze. For the embankment with 4 m in height, the mean skeleton stress did not reach zero and was maintained during the earthquake. Because of this stress behavior, the accumulated strain would not increase.

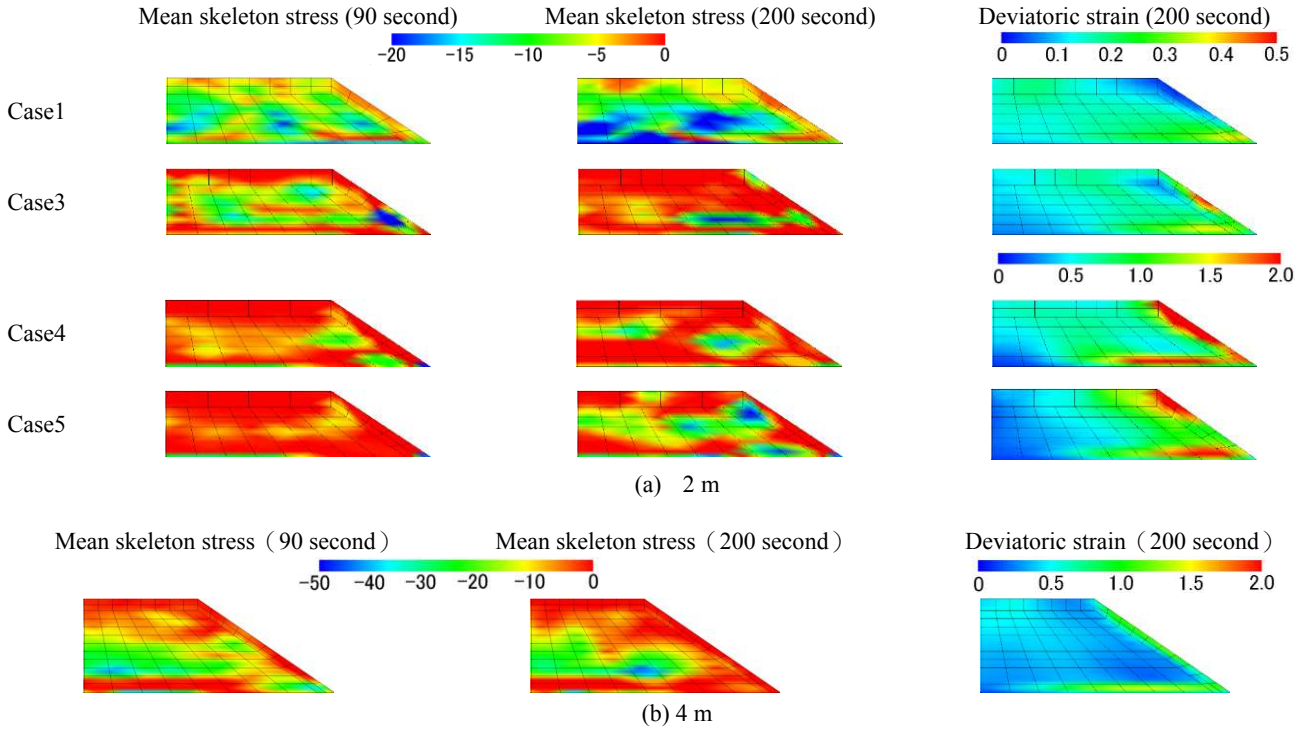

Figure 10. Distribution of mean skeleton stress and deviatoric strain

As shown in Figure 9, the differences of the residual deformation among five cases became larger in the simulation of the embankment with 2 m in height

5 CONCLUSIONS

In this paper, to clarify the dynamic behaviour of an embankment affected by the freeze and the thaw in snowy cold regions, series of numerical simulations were performed. For the numerical technique, the seepage-deformation coupled method was applied. In this technique, the three-phase porous media theory and conventional constitutive model for soil skeleton were adopted to describe the dynamic behaviour of unsaturated soil. In the series of simulations, the changes in the strength and the stiffness of the soil skeleton, the permeability of pore water and air, and boundary conditions for pore water and air, caused by the freeze and thaw were considered.

From the series of numerical simulations, it was revealed that the seismic resistance of the embankment affected by the thaw decreased as largely as that by severe rainfall. The degree of the influence was large in the low embankment because the decrease in the skeleton stress is observed in a lot of areas in the embankment.

6 ACKNOWLEDGEMENT

The authors would like to express their appreciation to the National Research Institute for Earth Science and Disaster Prevention for allowing the use of their K-NET record in this paper. This work was supported by JSPS KAKENHI Grant Numbers JP15K18111.

7 REFERENCES

Armstrong, P.J. & Frederick, C.O. 1966. *A mathematical representation of the multiaxial Bauschinger effect.* C.E.G.B. Report RD/B/N731.

Kawajiri, S., Suzuki, S., Tanaka, D., Kawaguchi, T., Nakamura, D. & Yamashita, S. 2016. Study on N_d - value of embankment affected by freeze-thaw and snowmelt water, *Proceedings of 49th Japanese National Conference of Geotechnical Engineering*, 725-726. (in Japanese)

Matsumaru, T. & Uzuoka, R. 2014a. Dynamic analysis of embankment based on three phase porous media theory using elasto-plastic constitutive mode for unsaturated soil. *Journal of Geotechnical Engineering (C)* 70(4): 395-411.

Matsumaru, T. & Uzuoka, R. 2014b. Three-phase coupled analysis of shaking table test of unsaturated embankment on inclined ground, *Proceedings of the 4th International Conference on Geotechnical Engineering for Disaster Mitigation and Rehabilitation*: 309-316.

Matsumaru, T., Uzuoka,R., Kiguchi, M. & Nishimura, T. 2015. Laboratory test and numerical study of cyclic behavior of unsaturated liquefiable sandy soil, *Proceedings of the 6th International Symposium on Deformation Characteristics of Geomaterials*, IS-Buenos Aires: 679-686.

Matsumaru, T. & Uzuoka, R. 2016. Three-phase seepage-deformation coupled analysis about unsaturated embankment damaged by earthquake. *International Journal of Geomechanics* 16(5): C4016006.

Morishima, H., Saruya, K. & Aizawa, F. 2005. Damage and reconstruction of the old railway at the section of structures using soil. *Foundation Engineering and Equipment* 33(10): 78–83 (in Japanese).

RTRI (Railway Technical Research Institute) 2007. The Design Standards for Railway Structures and Commentary (Earth structure), supervised by Ministry of Land, Infrastructure and Transport, Maruzen (in Japanese).

Sugii, T. (2002). Relationship between soil-water characteristic curve and void ratio. In *Proceedings of 3rd International Conference on Unsaturated Soils* 1: 209-214.

Uzuoka, R. & Borja R.I. 2012. Dynamics of unsaturated poroelastic solids at finite strain. *International Journal for Numerical and Analytical Methods in Geomechanics*, 36(13): 1535-1573.